11th International Symposium on Turbulence and Shear Flow Phenomena (TSFP11)
Southampton, UK, July 30 to August 2, 2019

ANALYSIS OF UNSTEADY FLOW IN OVEREXPANDED NOZZLE

Bakulu F., Lehnasch G., Goncalves da Silva E., Girard S., Jaunet V.
ISAE-ENSMA, Institut PPrime, Université de Poitiers, UPR 3346 CNRS
1 Avenue Clement Ader, 86000 Poitiers, France
florian.bakulu@ensma.fr

Herpe J.,
Direction des Lanceurs, Centre National d'Etudes Spatiales (CNES)
52 rue Hillairet, Paris, 75012, France
julien.herpe@cnes.fr

ABSTRACT

An over-expanded jet in a Truncated-Ideally Contoured (TIC) nozzle is investigated to identify the phenomena involved in the generation of lateral pressure forces. The operating conditions correspond to the generation of wall pressure fluctuations of maximal amplitude for the present geometry. Synchronized time-resolved velocity and wall pressure data are measured in planes normal to the jet axis downstream of the nozzle and along azimuthal rings of pressure sensors within the separated region in the nozzle. The first fluctuating modes of internal pressure and external velocity are found to be significantly correlated in a narrow frequency range. A Delayed Detached Eddy Simulation (DDES) is carried out to reproduce the global flow dynamics. It is shown in this case that lateral forces are dominated by the signature of this tonal behaviour.

1 Introduction

Nozzles operating at off-design conditions are likely to produce significant side loads, resulting from the unsteady non-axisymmetric flow motion. The features of lateral pressure forces vary as a function of the Nozzle Pressure Ratio (NPR) or the nozzle geometry. The present study focuses on Truncated Ideally Contour (TIC) nozzles for which only Free Shock Separation (FSS) regime is observed. In this case, the jet separates within the nozzle without reattachment. A separation shock is formed within the nozzle and leads to the apparition of a Mach disk followed by a subsonic flow at the core of the supersonic stream. The subsonic/supersonic co-flowing mixing layers present at the nozzle exit are surrounded by the separated region opening to the atmosphere downstream of the nozzle exit. This topology remains similar but progressively shifts downstream for increasing Nozzle Pressure Ratio (NPR). The unsteady flow behaviour observed in this regime has been related to various possible origins. For example, an upstream asymmetric laminar to turbulent transition has been observed at low NPR (Stark & Wagner (2009)). For higher NPR, the unsteadiness is instead related to the asymmetry of the separation line (Schmucker (1984)) and separation shock, or to the intermittency of the recirculation region due to the close proximity of the jet shear layer to the wall and subsequent pressure fluctuations in the back-flow region (Verma (2009)). The possible critical influence of the small vortex lip forming at the nozzle exit has also been suggested Georges-Picot *et al.* (2014) in FSS regime and different nozzle geometry. The nature of pressure fluctuations associated to these interrelated phenomena and their effective global contributions to the resulting wall pressure field yet still remains to be clarified.

The spatial and temporal structure of pressure fluctuations and their evolution with respect to NPR in TIC nozzle in FSS regime has recently been characterized by Jaunet *et al.* (2017). It was shown that the energy of pressure fluctuations exhibits a dominant bump at low Strouhal number regardless the NPR, which can be associated to the shock and separation line motion. Whereas this motion remains mainly axisymmetric, a lot of energy is also locally distributed among all the azimuthal modes. This motion has often been considered as being the main contribution to the generation of lateral forces. High-frequency contributions to the first azimuthal mode of wall pressure fluctuations may also be present. They can be associated to the signature of coherent structures spatially developing within the mixing layer, whose features depend on their size and their relative radial distance to the nozzle wall (thus on their relative distance from the separation line). The emergence of very distinct and energetic peaks of in the first and second azimuthal pressure modes in the middle frequency range has also been reported. In spite of their similarities with peaks reported by various authors in rather similar nozzle configurations, it was however shown that they could not be associated neither to transonic resonance (Zaman *et al.* (2002)), nor to classical screech mechanisms suggested by these authors. At this peak frequency, it was instead shown that a negative phase velocity of the first internal wall pressure mode appear as well as high amplitude of the transfer function between the pressure fluctuations towards the external velocity fluctuations. It has been thus suggested that the particular organization of wall pressure fluctuations may be mainly related in this case to intrinsic hydrodynamical instabilities developing in the downstream mixing layer.

The present study aims at examining more precisely the link between nozzle wall pressure and jet dynamics and its consequences on the generation of lateral forces. It re-

ports the analysis of experimental and numerical data which are both resolved in time and space so that the direct evaluation of coherence between the first azimuthal pressure and velocity modes can be carried out. Following the study of Jaunet *et al.* (2017), the present study focuses on the pressure operating conditions leading to pressure fluctuations of particularly great amplitude all along the nozzle and a clear emergence of a tonal peak in the first azimuthal fluctuating pressure mode.

The first section describes the experimental set-up. The numerical strategy adopted and its validation on this case are then presented. The common features and correlation between internal and external fluctuating fields are analyzed in the following sections. The last section is dedicated to the analysis of resulting lateral forces.

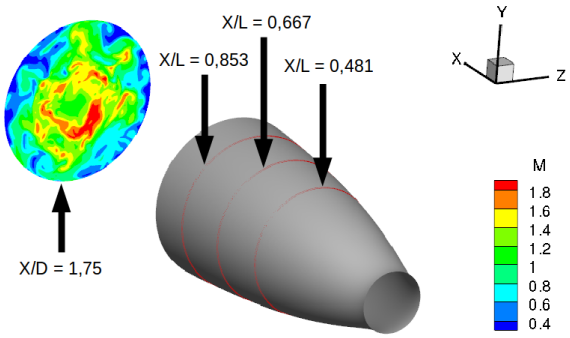

Figure 1. Position of the wall pressure sensors rings and PIV plane.

2 Experimental set-up

The experimental campaign is conducted in the S150 supersonic wind tunnel at Pprime Institute. A rigid subscale TIC nozzle is designed to reach a full-flowing flow condition with a Mach number $M = 3.5$. It is supplied with cold and desiccated air flow with low turbulence levels. In the following, U_j and D_j are the fully expanded jet velocity and jet diameter respectively corresponding to the fully expanded Mach number $M_j = 2.09$ selected for this study. These quantities are used to define non-dimensional time $t^* = tU_j/D_j$ and Strouhal number $St = fD_j/U_j$ based on time t or frequency f respectively.

Some synchronized PIV/wall pressure measurements are carried out. The locations of rings of wall pressure sensors and the external PIV plane are illustrated in figure 1. The nozzle is equipped with 18 flush-mounted Kulite XCQ-062 pressure transducers. These pressure sensors are distributed along 3 rings of 6 transducers placed equidistantly along the circumference. The first ring is located at $X/L = 0.481$, thus located close to the separation shock occurring at the middle of the nozzle in this case. The two other rings are in the recirculation zone at $X/L = 0.667$ and $X/L = 0.853$ where X is the axial distance from the nozzle throat and L is the divergent length. The pressure is measured during $10^5 t^*$ with a sample rate corresponding to $St = 20$. Stereo-PIV measurements are carried out with a diode pumped 527nm 30mJ Continuum MESA-PIV laser and high rate Photron cameras, and synchronized with the wall pressure acquisition system. The velocity data analyzed for this study are extracted in a plane normal to the jet axis and located at $x/D = 1.75$ where x and D are the axial distance from the nozzle exit and the nozzle exit diameter respectively. The magnitude of the transfer function from internal pressure fluctuations to external velocity fluctuations was previously evaluated in Jaunet *et al.* (2017). This position of the PIV plane is chosen so that it coincides to the region where some maximal values of the magnitude of this transfer function have been identified. It is assumed accordingly to help in improving the detection of coherence between internal and external fluctuating modes for the present study. PIV data are recorded during $2.1 \times 10^4 t*$ with a sample rate of $St = 1$.

3 Numerical set-up and verification

A Delayed Detached Eddy Simulation (DDES) is carried out for the corresponding TIC nozzle geometry and similar operating conditions. A wall condition is applied at the boundary surrounding the nozzle exit section instead of simulating the whole external nozzle geometry and the mesh is optimized in order to limit as far as possible the computational cost. The external cylindrical fluid domain downstream of the nozzle exit has a length of $28D$ and a radius of 5D. The mesh topology is splitted into thirteen subdomains in order to control grid clustering and orthogonality in near-wall and near-axis regions. It forms a cylindrical layer following the nozzle wall and extending within the jet downstream and an internal subdivision yielding a butterfly topology, as illustrated in figure 2. The distribution of points is set to satisfy mesh resolution requirements in both upstream attached boundary layer regions and the mixing region up to around one nozzle exit diameter downstream of the nozzle exit. The mesh is then progressively coarsened to limit the computational cost. The dimensionless wall distance is maintained below small values all along the nozzle wall in order to ensure the applicability of the wall law applied. The total number of points is about 49 millions.

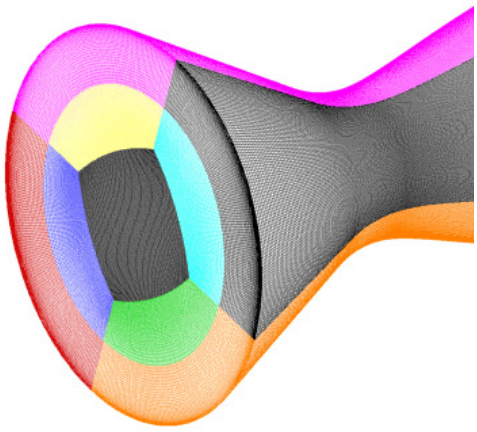

Figure 2. Illustration of the nozzle mesh topology

The in-house PHOENIX code developed at Pprime Institute is used. The methodology retained is similar to the one given by Goncalves *et al.* (2017).A dual time stepping implicit method is combined with a third order Runge-Kutta method for time integration. Inviscid fluxes are computed with second-order Jameson flux difference scheme for the averaged equations and with Roe flux difference scheme for the turbulence equations. The time

step is around $2.38 \times 10^{-2} t*$. The total physical time of the simulation is about $280 t*$.

The numerical results obtained are compared with the experimental results available for $M_j = 2.09$. The mean separation line is located at $X/L = 0.508$, very close to the reference experimental value $X/L = 0.495$. The distributions of average and fluctuating wall pressure along the nozzle are shown in figure 3. The Power Spectral Distributions (PSD) for the first azimuthal modes are also presented in figure 5 of next section (yet partially converged for the numerical results due to limited time of computation). The relative contribution of first mode appears exaggerated at low-frequencies in the simulation and as expected, the high-frequency contributions of higher modes are under-estimated due to the simulation of largest turbulent scales only. However, the salient peak of mode 1 in the intermediate frequency range, which is of main interest in the present study, appears well reproduced. These comparisons thus globally show that the present simulation strategy enables to capture both the statistical features of the pressure field and its main important dynamical features.

The comparison of experimental (from a former PIV campaign) and numerical streamwise velocity fields in figure 4 also shows that the expected external jet flow structure is quite well reproduced. The spreading of mixing layer downstream of the nozzle exit is yet slightly over-estimated due to the rapid mesh coarsening in the streamwise and radial directions in the external domain. This leads to a small shift of the jet flow structure (position of second Mach disk and subsequent compression/expansion regions) in the upstream direction. In the plane corresponding to the new PIV measurements at $X/D = 1.75$, the differences between predicted and measured average and rms velocity levels however remain typically less than 7% and 10% respectively. As a conclusion, even if the present numerical strategy admittedly leads to a limited representativity of the simulated external flow entrainment and far-field jet dynamics, the large scales dynamical features of the jet appear to be satisfactorily reproduced in the whole separated region and close to the nozzle exit.

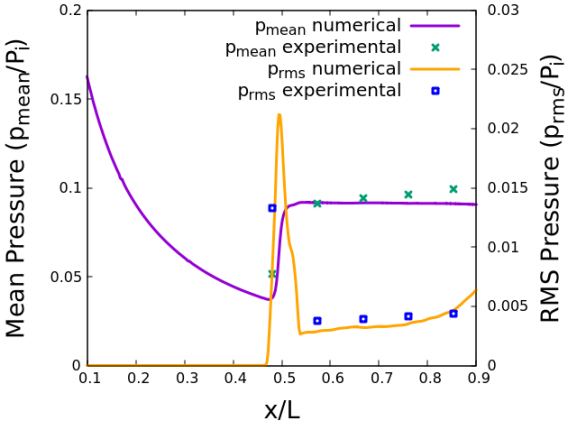

Figure 3. Average and RMS wall pressure distributions along the nozzle wall.

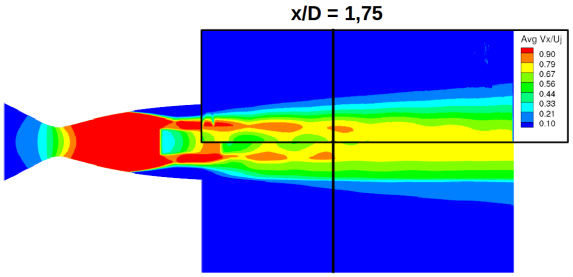

Figure 4. Average streamwise velocity field: reference x-y PIV data (surrounded by black rectangular box) versus overall numerical prediction. Position of the y-z cross-PIV plane (vertical black line).

4 Organization of internal wall pressure

The features of the fluctuating wall pressure field are first examined. For each ring of wall pressure sensors, the pressure field is decomposed into azimuthal Fourier modes

$$p_m(X,t) = \frac{1}{2\pi} \int_0^{2\pi} p(\theta,X,t) e^{-i\omega\theta} \mathrm{d}\theta$$

where m is the azimuthal mode number. The PSD of the 3 first modes evaluated at $X/D = 0.667$ are plotted for example in figure 5. The large low-frequency bump is visible on each distribution. This bump is all the more dominant as we consider a streamwise location close to the separation line and can be associated to the upstream shock motion. This large dominance of energy for $m = 0$ close to the separation line suggests that this shock motion mainly remains axisymmetric. Some significant fluctuating energy is also contained in the high-frequency range and increases as we move in the downstream direction. It can be attributed to the passage of smaller coherent structures advected along the separated region and jet mixing layer. Their contribution appear rather uniformly distributed in each azimuthal mode. The most salient feature is the presence of a peak of the antisymmetric mode $m = 1$ at $St \simeq 0.2$ in the middle frequency range. It should be recalled that this peak exists for all operating conditions but is more particularly dominant for $M_j = 2.09$. Other peaks at other frequencies can be detected for the other modes but remain of significantly lower amplitude.

The streamwise evolution of the pressure organization is further examined with the numerical simulation data. The PSD of the 3 first modes of the separation line position is presented for example in figure 6. The position of this separation line is detected based on a simple pressure gradient sensor at various azimuthal positions during the simulation. These PSD of separation line position naturally present strong similarities with the PSD of wall pressure modes previously evaluated experimentally downstream of the separation line. The dominant hump visible around $St \simeq 0.07$ for the mode $m = 0$ still confirms the existence of a dominant back and forth low-frequency displacement of the separation line and subsequent jet flow structure. It corresponds to the similar predominant energy bump of $m = 0$ wall-pressure mode that could recorded in any ring of sensors placed at the beginning of the separation zone. This axisymmetric motion is likely to produce significant thrust oscillations, yet without necessarily generating significant lateral forces. A distinct peak at $St \simeq 0.2$ is also still observed in the PSD of mode $m = 1$. This shows that the signa-

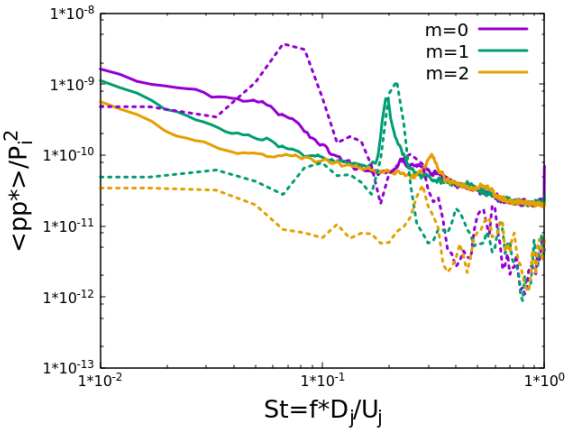

Figure 5. PSD of 3 first azimuthal pressure modes at X/L=0.667: experimental measurements (plain line) and numerical evaluation (dashed line).

ture of the resonance-like mechanism previously described is felt from the very beginning of the separated region.

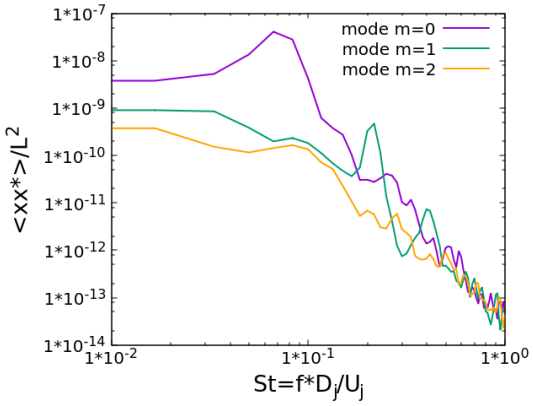

Figure 6. PSD of the 3 first azimuthal modes of the position of the separation line.

5 Links with the global flow organization

The present analysis is extended to the whole internal flow region based on numerical data. The PSD of the fluctuating pressure mode 1 is for example shown in figure 7 for the plane $X/L = 0.76$ (corresponding to the middle of the open separated region). As expected, some high levels of energy in a wide frequency range are observed between the radial positions $r/D = 0.2$ and 0.25. This zone corresponds to the mixing layer region spatially developing between the near axis subsonic jet core (downstream of the first internal Mach disk) and the external recirculation region. Whatever the radial position, a peak of energy also clearly emerges at $St \simeq 0.2$. This result thus indicates that the particular wall pressure field organization previously observed is not confined to the near-wall region. It rather appears as the signature of a more global flow organization of the pressure field prevailing through the whole separated flow region within the nozzle. The maximal energy levels are located within the mixing layer, more particularly close to the internal part of the mixing layer (at $r/D \simeq 0.215$) for this streamwise location. This highlights the probable prominent role of intrinsic non-axisymmetric instabilities spatially developing within the jet mixing layer inside the nozzle.

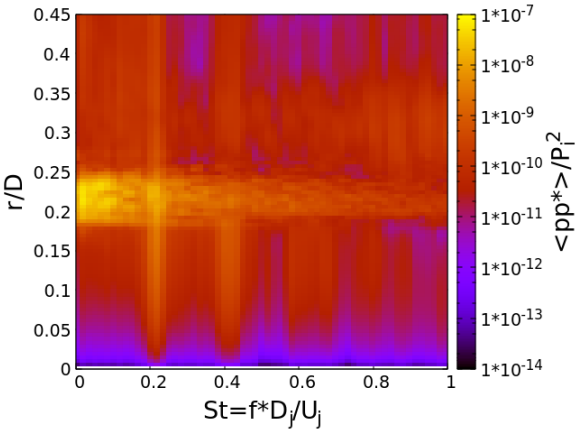

Figure 7. PSD map of the azimuthal pressure mode $m = 1$ in the plane at X/L=0.76 as a function of the radius.

The organization of the velocity field downstream of the nozzle exit and its link with the internal wall pressure field are now examined. The structure of velocity field at the level of the PIV plane is first briefly described. The overall flow visualization given by figure 4 indicates that a second Mach disk forms just downstream of the nozzle exit and is followed by subsequent expansion/compression zone. The PIV plane at $x/D = 1.75$ is located close to the end of the pseudo-potential core slightly before the internal part of the mixing layer reaches the jet axis. In this region, a deficit of velocity could be still observed near the jet center in the radial profile of mean streamwise velocity. The mixing region roughly extends from $r/D = 0.2$ to 0.6. It is composed of two distinct mixing regions: *i/* an internal mixing layer issued from the triple point connected to the separation shock and first Mach disk within the nozzle and *ii/* an external mixing layer between the surrounding supersonic coflow and the recirculation zone. Higher values of RMS velocity are naturally observed in this region with a peak value found near $r/D = 0.33$, which corresponds to the merging zone between these internal and external mixing layers. In order to analyze the azimuthal organization of the fluctuating velocity field in this plane, velocity data are interpolated on a cylindrical mesh with a resolution of 120 points in the azimuthal direction before applying the Fourier spatio-temporal decomposition. As expected for such a position located quite far downstream, the results show that the fluctuating energy within the whole mixing region is distributed into a large number of azimuthal modes and within a large frequency range. However, as shown in figure 8, a small peak still clearly emerges at $St \simeq 0.2$ in the PSD of first azimuthal mode of velocity. It is more particularly visible near $r/D = 0.33$ where the merging between the internal and external mixing layers is observed and where the maximal rms values are detected. The amplitude of this energy peak of first mode of velocity field is here far lower than the one of first azimuthal pressure mode of the internal wall pressure signals. It remains however sufficiently significant to suggest that the turbulent structures spatially developing within the jet mixing layers also exhibit the same signature of a common global oscillation mechanism.

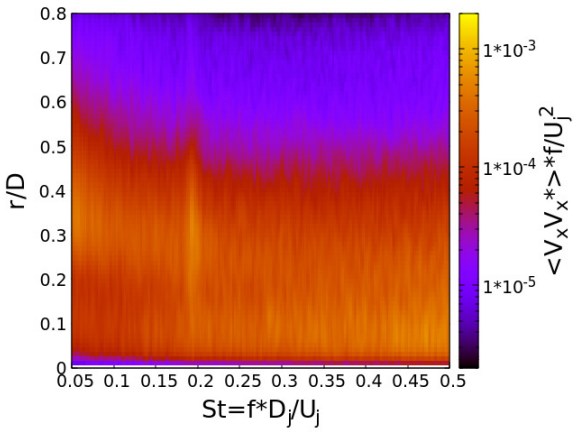

Figure 8. Pre-multiplied PSD of the anti-symmetric azimuthal mode in function of the radius and the Strouhal number at the plane $x/D = 1.75$.

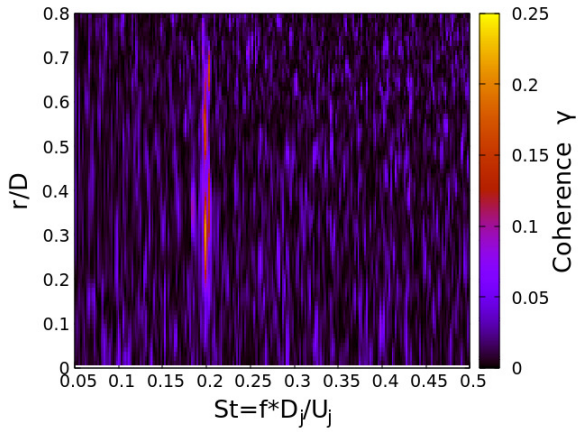

Figure 9. Coherence map between anti-symmetric azimuthal modes $m = 1$ of wall pressure signals (at $X/L = 0.481$) and jet velocity (at $x/D = 1.75$).

Synchronized and time-resolved data of wall pressure and external velocity have been obtained during a time period long enough to allow an extended correlation analysis based on experimental measurements. A low-pass filtering of wall pressure data is first applied in order to obtain pressure and velocity signals with similar sample rate. The coherence between the first azimuthal modes of internal pressure at a ring of wall pressure sensors and first azimuthal mode of streamwise velocity is computed. The coherence map obtained remains rather similar whatever the pressure ring position considered. The map obtained for the ring of sensors at $X/L = 0.481$ and the PIV plane at $x/D = 1.75$ is for example presented in figure 9. As expected, the signals are uncorrelated at nearly all frequencies due to the important distance between the internal sensors and the external velocity plane. However, a significant coherence level emerges at $St = 0.2$ and more particularly close to $r/D = 0.33$ in the external velocity plane and to a lower extent close to $r/D = 0.51$. As previously mentioned, this first position corresponds to the zone where the internal and external mixing layers start merging. The second outer position is close to the boundary of the external mixing layer. In spite of high-amplitude and stochastic turbulent fluctuations found within the jet at such a quite far downstream position, the existence of such a peak of coherence reveals that first modes of internal pressure fluctuations and external velocity fluctuations remain significantly correlated but only in a narrow middle frequency range. The non-axisymmetric modes of internal pressure field and the external jet velocity field thus share the common signature of an organized coherent motion in this particular narrow frequency range.

6 Lateral pressure forces

The aerodynamical forces resulting from the particular flow organization previously described are finally examined based on numerical data. The streamwise distribution of RMS of linear forces (force per unit length) components is first presented in figure 10 where $F_{ref} = P_\infty \pi D^2/4$ and where the local contribution of force components per unit length f_x, f_y and f_z are expressed in the general coordinate system with x the streamwise direction and y and z the radial directions. At each streamwise location within the nozzle, this is evaluated by integrating the force over the whole circumference and over the local mesh size in the streamwise direction and dividing by this size. The statistical distribution of the unsteady local lateral forces generated as a function of the position along the nozzle can be thus here examined by considering the combined effect of both the evolution of the force amplitude and the surface over which they are applied. Due to limited time of computation, it is admittedly not sufficiently converged to give any accurate quantitive estimate of the effective levels of forces that may be encountered. However, it already clearly highlights how the lateral forces are organized along the nozzle. As expected, a first dominant source of lateral forces is located in close proximity to the separation line where the higher local levels of streamwise pressure gradients are encountered. This corresponds to a source of lateral force commonly suggested in the litterature. In the present case, this source does not yet appear as dominant as in other studies. A secondary dominant local peak of lateral force is also observed close to the nozzle exit while a quite uniform region of significant RMS levels (typically greater than 50% of the peak levels) is found all along the separated region.

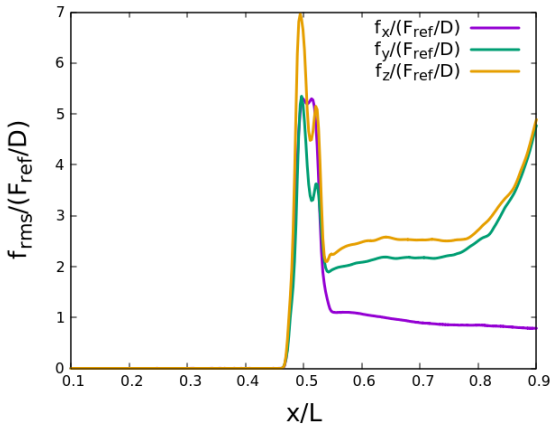

Figure 10. Streamwise linear distribution of RMS of forces components.

The time evolution of the global force integrated all along the nozzle divergent is finally computed to examine

the resulting spectral properties of each force component. The PSD of each force component is reported in figure 11. The hump around $St = 0.07$ in the PSD of F_x can be related to the global axisymmetric motion of the upstream separation line previously presented. It should be reminded that rather low-frequency contributions to lateral forces are more often reported in other studies corresponding to separated jets without any clear tonal behaviour. Such low-frequency components are thus often associated only with dominant low-frequency shock motions for all modes. The most original observation in the present study is the emergence of the dominant peak also for lateral forces around $St = 0.2$. This result thus contrasts with other results in the literature. Only moderate fluctuating energy levels of pressure mode $m = 1$ are thus observed locally within the flow. However, their coherence in the streamwise direction appears sufficiently important to lead to a dominant contribution to lateral forces.

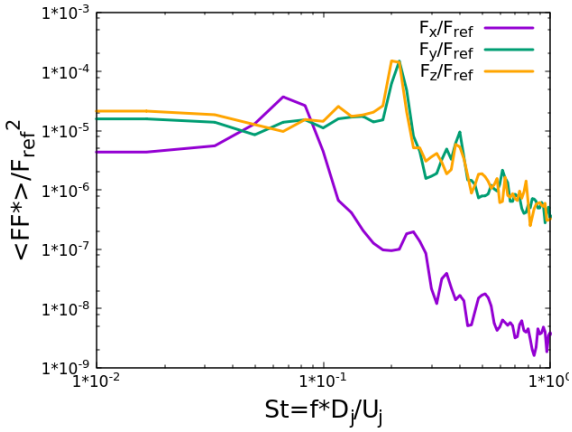

Figure 11. PSD of the global aerodynamic forces F_x, F_y and F_z.

7 Conclusions and perspectives

The unsteady features of a separated supersonic jet in a TIC nozzle have been investigated for a nozzle pressure ratio corresponding to wall pressure oscillations of maximal amplitude. The wall pressure field shows signs of a particular tonal behaviour which has been previously reported. This study has focused on a new correlation analysis of synchronized time-resolved external velocity and internal wall pressure data to further understand the possible link existing between internal and external disturbances. In a narrow frequency band, a significant coherence level has been found between the non-axisymmetric internal wall pressure oscillations prevailing in the nozzle and non-axisymmetric external velocity disturbances spatially evolving in the jet mixing layer quite far downstream of the nozzle exit. The possible emergence of a global resonance mechanism is also further ascertained through the highlighting of such peaks of non-axisymmetric pressure fluctuations within the whole extent of the separated region. The flow behaviour has been numerically reproduced by DDES and validated with the available experimental results, allowing an evaluation of the subsequent lateral forces applying to the nozzle. Despite relatively moderate local energy levels of the first azimuthal mode of wall pressure in this frequency range, it has been shown that these tonal jet oscillations fully dominate the whole dynamical behaviour of these lateral forces. These findings clearly suggest that any modification of the external jet environment is likely to affect not only the intrinsic external jet dynamics but also the side-loads features.

Acknowledgments

The present work is part of the PhD Thesis of Florian Bakulu, supported by CNES and Région Poitou-Charentes. This work was granted access to the HPC resources of TGCC under the allocation A0032A10017 made by GENCI.

REFERENCES

Georges-Picot, A., Hadjadj, A. & Herpe, J. 2014 Influence of downstream unsteadiness on shock pattern in separated nozzle flows. In *50th AIAA/ASME/SAE/ASEE Joint Propulsion Conference*, p. 4000.

Goncalves, E., Lehnasch, G. & Herpe, J. 2017 Hybrid rans/les simulation of shock-induced separated flow in truncated ideal contour nozzle. In *International Symposium on Shock Waves*, pp. 507–513. Springer.

Jaunet, V., Arbos, S., Lehnasch, G. & Girard, S. 2017 Wall pressure and external velocity field relation in overexpanded supersonic jets. *AIAA Journal* pp. 4245–4257.

Schmucker, R.H. 1984 Flow processes in overexpanded chemical rocket nozzles. part 2 : side loads due to asymmetric separation. *Tech. Rep.* NASA TM-77395.

Stark, R. & Wagner, B. 2009 Experimental study of boundary layer separation in truncated ideal contour nozzles. *Shock Waves* **19** (3), 185–191.

Verma, S.B. 2009 Shock unsteadiness in a thrust optimized parabolic nozzle. *Shock Waves* **19** (3), 193–212.

Zaman, K.B.M.Q., Dahl, M.D., Bencic, T.J. & Loh, C.Y. 2002 Investigation of a transonic resonance with convergent-divergent nozzles. *Journal of Fluid Mechanics* **463**, 313–343.